J Geod (2012) 86:165–180
DOI 10.1007/s00190-011-0506-7

ORIGINAL ARTICLE

The US Gravimetric Geoid of 2009 (USGG2009): model development and evaluation

Y. M. Wang · J. Saleh · X. Li · D. R. Roman

Received: 29 November 2010 / Accepted: 1 August 2011 / Published online: 17 September 2011

Abstract A new gravimetric geoid model, USGG2009 (see Abbreviations), has been developed for the United States and its territories including the Conterminous US (CONUS), Alaska, Hawaii, Guam, the Commonwealth of the Northern Mariana Islands, American Samoa, Puerto Rico and the US Virgin Islands. USGG2009 is based on a $1' \times 1'$ gravity grid derived from the NGS surface gravity data and the DNSC08 altimetry-derived anomalies, the SRTM-DTED1 $3''$ DEM for its topographic reductions, and the global geopotential model EGM08 as a reference model. USGG2009 geoid heights are compared with control values determined at 18,398 Bench Marks over CONUS, where both the ellipsoidal height above NAD 83 and the Helmert orthometric height above NAVD 88 are known. Correcting for the ellipsoidal datum difference, this permits a comparison of the geoid heights to independent data. The standard deviation of the differences is 6.3 cm in contrast to 8.4 cm for its immediate predecessor—USGG2003. To minimize the effect of long-wavelength errors that are known to exist in NAVD88, these comparisons were made on a state-by-state basis. The standard deviations of the differences range from 3–5 cm in eastern states to about 6–9 cm in the more mountainous western states. If the GPS/Bench Marks-derived geoid heights are corrected by removing a GRACE-derived estimate of the long-wavelength NAVD88 errors before the comparison, the standard deviation of their differences from USGG2009 drops to 4.3 cm nationally and 2–4 cm in eastern states and 4–8 in states with a maximum error of 26.4 cm in California and minimum of −32.1 cm in Washington. USGG2009 is also compared with geoid heights derived from 40 tide-gauges and a physical dynamic ocean topography model in the Gulf of Mexico; the mean of the differences is 3.3 cm and their standard deviation is 5.0 cm. When USGG2009-derived deflections of the vertical are compared with 3,415 observed surface astro-geodetic deflections, the standard deviation of the differences in the N–S and E–W components are $0.87''$ and $0.94''$, respectively.

Keywords Gravimetric geoid · Gravity anomaly · Helmert condensation · Terrain correction · Harmonic continuation

Abbreviations

CONUS	The Conterminous US
NOAA	National Oceanic and Atmospheric Administration
GSFC	Goddard Space Flight Center
NGA	National Geospatial Agency
NGS	National Geodetic Survey
DNSC	Danish National Space Center
SIO	Scripps Institute of Oceanography
GPS	Global Positioning System
SRTM	Shuttle Radar Topography Mission
GRACE	Gravity Recovery and Climate Experiment
GOCE	Gravity and Ocean Circulation Explorer
NAVD88	North American Vertical Datum of 1988
NAD83	North American Datum 1983
NSRS2007	National Spatial Reference System of 2007
EGM08	Earth Gravitational Model of 2008
EGM96	Earth Gravitational Model of 1996

Y. M. Wang (✉) · D. R. Roman
National Geodetic Survey, Silver Spring, MD, USA
e-mail: Yan.Wang@noaa.gov

J. Saleh · X. Li
ERT Inc., Silver Spring, MD, USA

GGM	Global Gravity Model
USGG2009	The US Gravimetric Geoid of 2009
USGG2003	The US Gravimetric Geoid of 2003
GRAV-D	Gravity for the Redefinition of the American Vertical Datum
DTED	Digital Terrain Elevation Data
NED	National Elevation Dataset
DOT	Dynamic Ocean Topography
DEM	Digital Elevation Model
BM	Leveling Bench Mark
GPSBM	Leveling Bench Marks with GPS heights
MSL	Mean Sea Level
1D FFT	1 Dimensional Fast Fourier Transform
TC	Terrain Correction
RTM	Residual Terrain Model

1 Introduction

NOAA's National Geodetic Survey (NGS) has been developing geoid models for the United States for two decades starting with GEOID90 (Milbert 1991; Smith and Milbert 1999; Smith and Roman 2001; Roman et al. 2004). This paper describes the most recent model of this series: USGG2009.

The computation of USGG2009 was motivated by several recent developments. For the first time, the long-wavelength portion of the gravity field has been captured very accurately by the satellite Gravity Recovery and Climate Experiment (GRACE) mission and can be accessed through low degree geopotential models such as GGM02 (Tapley et al. 2005) and GGM03. The ultra-high resolution geopotential model EGM08 (Pavlis et al. 2008) has become available. The Shuttle Radar Topography Mission (SRTM) DEM has become publicly accessible for most of the North American continent on a 3″ grid (Slater et al. 2006). Finally, the NAD 83(NSRS2007) national readjustment changed the ellipsoidal heights in the NGS database by several centimeters in some states and improved the accuracy and consistency of the ellipsoidal heights at 67,693 stations distributed all over CONUS (Pursell and Potterfield 2008). This collection of new results called for a new geoid model.

Past NGS gravimetric geoid models were computed using the Faye anomaly, which is based on the terrain correction, as an approximation of Helmert's anomaly on the geoid. These models combined the Faye anomaly with global reference geopotential models in a standard remove-restore fashion. The topographic and gravity reductions of such a geoid computation procedure involve several approximations. In addition, the effect of the long-wavelength errors of the surface gravity data on the gravimetric geoid was neither eliminated nor minimized. Since these weaknesses can no longer be tolerated in the computation of a modern, centimeter-accurate geoid, USGG2009 is computed differently.

The long-wavelength content of USGG2009 is based on a contribution from GRACE rather than the surface gravity data. Its gravity and topography reductions are based on the harmonic continuation method rather than the traditional approximation of Helmert's second condensation by using the terrain correction. Harmonic continuation is the method that underlies modern global geopotential models such as EGM08. Therefore, it is much easier to compute a geoid with this method rather than the approximate (Faye anomalies) or even the rigorous Helmert's second condensation. We did, however, compute a geoid based on the latter method, using the SRTM-DTED1 3″ DEM for terrain correction computations, for comparison with USGG2009 and its validation. This paper describes the data and computational methods used to develop USGG2009 and several tests for its evaluation.

2 USGG2009 computation methods

Helmert's second method of condensation has been thoroughly investigated, as is evident by the abundance of papers in the geodetic literature (Moritz 1968; Vaníček and Kleusberg 1987; Wang and Rapp 1990; Martinec et al. 1993; Vaníček and Martinec 1994; Martinec 1998; Sjöberg 2000 and Heck 2003). Alternatively, the geoid could be computed by harmonic downward continuation (Bjerhammar 1963; Sjöberg 1977, 2001, 2003, 2007; Wang 1990, 1997). We used the latter method to compute USGG2009. It is more suitable for use with modern ultra-high degree reference geopotential models such as the EGM08, since it is used in their computation.

Each of these methods deals with the topographic and gravity reductions and the reference geopotential models differently. However, if both are computed rigorously they should result in almost identical geoid models. These two methods are described, respectively, in the following subsections.

2.1 Helmert's second condensation

The geoid may be computed by the Stokes' integral. Before this integral can be accurately used, the masses above the geoid should be removed in order to satisfy the harmonic requirement of Stokes' problem (Heiskanen and Moritz 1967). Helmert's second method of condensation does that by condensing the topographic masses onto the geoid in an infinitely thin mass layer. The resulting "Helmert anomaly" on the Earth surface, Δg_S^H, is defined by subtracting the direct

effect, A, from the atmospherically corrected surface free-air gravity anomaly Δg (computed using orthometric rather than normal heights):

$$\Delta g_{\mathrm{s}}^{H} = \Delta g - A \tag{1}$$

The direct effect is the difference between the attraction of the actual topography and that of its condensed layer on the geoid. An algorithm for computing the direct effect is derived in the appendix, based on a spherical harmonic expansion of the topography to degree and order 2160 (see A20). A constant topographic density of 2.67 g/cm^3 is used throughout this work.

It is a common practice in local geoid computations to use a global geopotential model as a "reference model", in combination with the surface gravity data. If the accurate long-wavelength contribution of GRACE is to be adopted, the reference model must be compatible with the surface gravity data. In Helmert's second condensation, the two are compatible if they are defined in Helmert's space (Vaníček et al. 1996). Converting the reference model into Helmert's space could be done using a spherical harmonic expansion of the topography to the same maximal degree and order as the reference model. This expansion is then used to form two additional spherical harmonic expansions: one for the gravitational potential of the actual topography and another for that of the condensed layer on the geoid. The difference between these two potentials is denoted by δV^{e}. The reference geopotential model is converted into Helmert's space, hereafter called "Helmertized", by subtracting from its harmonic coefficients those of δV^{e}. A spherical harmonic representation of δV^{e} is derived in the appendix and its final form is given in Eq. A19.

The residual Helmert anomaly on the Earth surface, $\mathrm{d}\Delta g_{\mathrm{S}}$, is then computed by

$$\mathrm{d}\Delta g_{\mathrm{S}} = \Delta g_{\mathrm{S}}^{H} - \Delta g_{\mathrm{Ref}}^{H} \tag{2}$$

where $\Delta g_{\mathrm{Ref}}^{H}$ is the reference Helmert gravity anomaly on the surface, computed using the "Helmertized" reference model.

The surface Helmert anomaly residual must now be reduced to the geoid. This residual is small if the reference model is used to a high degree and order. Therefore, its downward continued value on the geoid, $\mathrm{d}\Delta g_g$, may be computed using the simple first order Taylor expansion:

$$\mathrm{d}\Delta g_{\mathrm{g}} \approx \mathrm{d}\Delta g_{\mathrm{S}} - \frac{\partial(\mathrm{d}\Delta g)}{\partial H} H \quad . \tag{3}$$

We will return to the downward continuation operation later in this section. The geoid is now computed using the remove-restore technique, by

$$N = N_{\mathrm{Ref}} + \frac{R}{4\pi\gamma} \int\int_{\sigma} \mathrm{d}\Delta g_{\mathrm{g}} S(\psi) \mathrm{d}\sigma \tag{4}$$

where, according to Helmert's theory, the reference geoid height, N_{Ref} in (4), should be computed by

$$N_{\mathrm{Ref}} = N^{H} + \delta N_{\mathrm{Ind}}. \tag{5}$$

The quantity N^H in (5) is the geoid in Helmert's space as computed from the "Helmertized" reference model, while δN_{Ind} is the indirect effect, i.e., the difference between the potential of the actual topography and that of the condensed layer on the geoid, divided by the normal gravity. This quantity is derived in the appendix, based on a spherical harmonic expansion of the topography, and given in Eq. A23.

The computations involved in Eqs. (2) and (5) are done without any spherical assumptions. Thus the ellipsoidal correction is already included in N_{Ref} and $\Delta g_{\mathrm{Ref}}^{H}$ to the maximal degree used in the computations. If the maximal degree is 360 or higher, the remaining power of the geoid, given in the second term on the right-hand side of Eq. (4), is on the decimeter level or less. Since the corresponding ellipsoidal correction is of the order of 1 mm, we neglect it and do not discuss it any further.

In practice, the integration in (4) is evaluated locally, over a rectangular or a spherical cap. To prevent the long-wavelength errors of the surface gravity data from leaking into the residual geoid, we adopt the kernel modification method of Wong and Gore (1969). The Stokes' kernel in (4) is replaced by a truncated one:

$$N = N_{\mathrm{Ref}} + \frac{R}{4\pi\gamma} \int\int_{\sigma_0} \mathrm{d}\Delta g_{\mathrm{g}} S^{H}(\psi) \mathrm{d}\sigma \tag{6}$$

where σ_0 is the integration area in which surface gravity is available, and S^H is the truncated Stokes kernel, defined as

$$S^{H}(\psi) = S(\psi) - \sum_{n=2}^{M} S_n(\psi) = \sum_{n=M+1}^{\infty} S_n(\psi) \tag{7}$$

where M is the cut-off or truncation degree (we used $M = 120$), $S(\psi)$ is the Stokes' function and

$$S_n(\psi) = \frac{2n+1}{n-1} P_n(\cos\psi), \tag{8}$$

where P_n is the Legendre polynomial of degree n.

The use of the truncated Stokes kernel guarantees that the long-wavelength ($n \le M$) content of the surface gravity data is not allowed to contribute to Stokes' integral. Rather, these long wavelengths are exclusively contributed by the global geopotential model through N_{Ref}. The higher frequency spectrum of the field, however, is still contributed by the surface gravity data in the second term on the right-hand side of (6). This method or its variations are favorable nowadays since modern reference geopotential models, such as EGM08, have very accurate long-wavelength content (cumulative error of 7 mm to degree and order 70) and therefore

should replace the surface gravity data in defining the long and medium wavelengths of the geoid.

Let us return to the downward continuation operation. The vertical gradient of the residual anomaly, in Eq. (3), can be computed by (Moritz 1980, p. 384):

$$\frac{\partial(\mathrm{d}\Delta g)}{\partial H}_{p} = \frac{R^2}{2\pi}\int\int_{\sigma}\frac{\mathrm{d}\Delta g - \mathrm{d}\Delta g_P}{l^3}\mathrm{d}\sigma \approx \frac{R^2}{2\pi}\int\int_{\sigma_0}\frac{\mathrm{d}\Delta g - \mathrm{d}\Delta g_P}{l^3}\mathrm{d}\sigma, \quad (9)$$

where l is the horizontal distance between the computation point P and the integration element, $\mathrm{d}\sigma$.

Let the residual geoid integral in Eq. (6) be denoted by $\mathrm{d}N$, and substitute (3) in $\mathrm{d}N$ to get

$$\mathrm{d}N \approx \frac{R}{4\pi\gamma}\int\int_{\sigma_0}\left[\mathrm{d}\Delta g_{\mathrm{S}} - \frac{\partial(\mathrm{d}\Delta g)}{\partial H}H\right]S^H(\psi)\mathrm{d}\sigma \equiv \mathrm{d}N^H + \mathrm{d}N_{\mathrm{DWC}} \quad (10)$$

where

$$\mathrm{d}N^H \approx \frac{R}{4\pi\gamma}\int\int_{\sigma_0}\mathrm{d}\Delta g_{\mathrm{S}}S^H(\psi)\mathrm{d}\sigma \quad (11)$$

$$\mathrm{d}N_{\mathrm{DWC}} \approx -\frac{R}{4\pi\gamma}\int\int_{\sigma_0}\frac{\partial(\mathrm{d}\Delta g)}{\partial H}HS^H(\psi)\mathrm{d}\sigma \quad (12)$$

The index "DWC" in Eqs. (10) and (12) stands for "downward continuation". So instead of actually downward continuing the residual gravity anomalies to the geoid with Eqs. (3) and (9), one could use the surface residual anomalies in Stokes' integral as in (11), but correct the so-obtained geoid residuals by adding a geoid correction computed using Eq. (12). If an ultra high degree and order reference model such as EGM08 is used, the residual field is so small ($\sim$ 2.5 mGal in the CONUS) that the integral (12) is at the 1 mm level except in the Rocky Mountains, where it could reach 6 cm. When compared with a nationwide set of GPS Bench Marks, the correction changed the RMS differences by 2–4 mm in mountainous states like Colorado and Idaho, but had almost no effect in most other states.

The Faye anomaly represents a simplification of Helmert's second method of condensation. The Faye anomaly is obtained from the surface free-air gravity anomaly by adding the classic terrain correction:

$$\Delta g_{\mathrm{g}}^H \approx \Delta g + \mathrm{TC} \quad (13)$$

where TC is given by Moritz (1980, p. 415):

$$\mathrm{TC} = \frac{1}{2}G\rho R^2\int\int_{\sigma}\frac{(H-H_P)^2}{l^3}\mathrm{d}\sigma \quad (14)$$

Notice that Δg_{g}^H refers to the geoid while the surface gravity anomaly, Δg, and TC are computed at the gravity point on the Earth surface.

2.2 Harmonic downward continuation

In this method, the surface free-air anomaly is compatible with the global reference model without any manipulations of the latter. The residual surface free air gravity anomaly is computed by

$$\mathrm{d}\Delta g_{\mathrm{S}} = \Delta g - \Delta g_{\mathrm{Ref}} - \Delta g_{\mathrm{RTM}} \quad (15)$$

where Δg_{Ref} is the reference free-air anomaly, synthesized from the reference model on the Earth surface, and where Δg_{RTM} is the surface gravity anomaly computed from a residual terrain model (Forsberg 1984). If the reference model is used to a high degree and order, this residual surface anomaly is small and can be downward continued to the geoid using Eq. (3). However, instead of the actual downward continuation of the surface residual anomaly to the geoid, the geoid correction (Eq. 12) accounts for our use of $\mathrm{d}\Delta g_{\mathrm{S}}$ in place of $\mathrm{d}\Delta g_{\mathrm{g}}$ in Eq. (6). The term $\mathrm{d}N_{\mathrm{DWC}}$ is added to Eq. (6), where the reference geoid height is given by (Wang 1990; Sjöberg 2007)

$$N_{\mathrm{ref}} = \zeta_{\mathrm{Ref}} + \gamma^{-1}\delta V_b + \zeta_{\mathrm{RTM}} \quad (16)$$

and where δV_b is the difference between the true potential of the topography and the harmonic downward continued one on the geoid. It is the so-called "analytical downward continuation error" (Sjöberg 1977; Wang 1997), renamed by Sjöberg (2007) to the "topographic bias". Equations for its computation are derived in the appendix and Eq. A24 gives δV_b in the form of a spherical harmonic series. The quantity ζ_{Ref} in (16) is the reference height anomaly, synthesized from the reference model on the geoid. Finally, ζ_{RTM} is the RTM effect on the geoid, added to restore the topographic contributions to compensate for the removal operation in Eq. (15).

3 Data and computation

About 1.5 million terrestrial and shipborne gravity data points in the US, Canada and Mexico are used for developing USGG2009. In addition, the DNSC08 satellite altimetry-derived gravity anomalies (Andersen and Knudsen 2009) are used. Two other altimetry-derived models, SIO/NOAA 2008 (Sandwell and Smith 2009) and GSFC00.1 (Wang 2001), are also tested and their performance compared with DNSC08. The DNSC08 and SIO/NOAA data perform very similarly. Both are significantly better than GSFC00.1 in northeast CONUS and slightly better in the Gulf of Mexico. GSFC00.1

performs significantly better in southeast CONUS to the Mid-Atlantic States. All models perform similarly on the west coast of CONUS. When altimetry-derived gravity in a 50 km strip near-shore is not used, the geoid improves very slightly.

The SRTM-DTED1 elevations were obtained from the National Geospatial Agency (NGA) over the window $\{10^\circ \leq \text{lat} \leq 60^\circ; 190^\circ \leq \text{long} \leq 308^\circ\}$, in the form of several thousand $1^\circ \times 1^\circ$ gridded tiles. The cell sizes of these grids are $3'' \times 3''$ below latitude 50° and $3'' \times 6''$ above it. Two large tiles were assembled: one above and the other below latitude 50°. These tiles contained over 12 million voids, several of which are of the size of a large county in the U.S. To fill these voids and verify quality, another continental-scale DEM was assembled using the National Elevation Database (NED) from the U.S. Geological Survey and the National Canadian and the National Mexican DEMs. These DEMs come in thousands of tiles of different sizes and data intervals, some in grid and others in raster (cell center) formats. All tiles were re-sampled on $3'' \times 3''$ cell grids and "mosaiced" to form the "National DEM", independent of SRTM. Voids above latitude 50° in SRTM-DTED1 were then filled and tiles re-sampled in $3'' \times 3''$ cells in the window $\{50^\circ \leq \text{lat} \leq 60^\circ; 190^\circ \leq \text{long} \leq 308^\circ\}$. Voids below latitude 50° were filled and the resulting $\{10^\circ \leq \text{lat} \leq 50^\circ; 190^\circ \leq \text{long} \leq 308^\circ\}$ window "mosaiced" with the previous one to create a North/Central American $3''$ SRTM DEM. Once the quality of this DEM was verified by comparison with the National DEM, it was used to compute all topographic reductions necessary for creating USGG2009. These include the terrain correction, which goes into the approximation of the Helmert second condensation geoid, and the Residual Terrain Model (RTM) (Forsberg 1984) effects, which go into several tests of the harmonic continuation geoid.

Residual gravity anomalies with respect to the full power of EGM08 are computed on the Earth surface. The RMS value of these residuals is 16.3 mGal for land data, 4.3 mGal for ship gravity, 1.5 mGal for the altimetry-derived data and 5.3 mGal for all data. When the RTM gravity effects due to the $3''$ SRTM-DTED1 with respect to a $5'$ mean topography are removed from the land gravity residuals, their RMS decreased from 16.3 to 5.1 mGal and the RMS value of all residuals reduced to 2.9 mGal. The RTM effect is computed based on the flat-top prism integration method using program TC (Forsberg 1984) and an integration radius of 50 km. No coarse DEM was used in the RTM computation. Residuals larger in absolute value than three-sigma are rejected. Residuals that pass this editing criterion are gridded by a weighted mean of the nearest neighbors with weights inversely proportional to the square of their distance from the computation point.

USGG2009 is then computed based on the harmonic continuation method, according to steps outlined in the earlier section. The gridded residuals are inserted into Stokes' integral using a modified Stokes' kernel according to Wong and Gore with degrees 2 to 120 set to zero. We tested several other cut-off degrees, but found 120 to be optimal. All integrations are computed using 1D FFT (Haagmans et al. 1993).

The north-south and east-west slopes of the gravimetric geoid are computed by bi-cubic splines and used to compute deflections of the vertical (DOV) on the geoid. To facilitate comparisons to a nationwide set of astro-geodetic deflections, the DOVs on the geoid are upward continued to the Earth surface by applying the correction due to the curvature of the plumb-line (Heiskanen and Moritz 1967). The horizontal derivatives of the topography for the plumb-line corrections are computed using a 1×1 min mean DEM (Smith and Roman 2001).

Five additional datasets served for testing the geoid models:

1. GPS Bench Marks (GPSBMs), which include 18,972 GPS-occupied Bench Marks in the US and Canada, selected out of 20,446 available GPSBMs (Fig. 1). Some GPSBMs were rejected either due to their poor ellipsoidal height accuracy, extreme deviation from USGG2009, subsidence in the vicinity of the GPSBM, or advice from NGS geodetic advisors assigned to many of the U.S. states.
2. An estimate of the long-wavelength errors of the US vertical datum, NAVD88 (Fig. 2), was computed as follows. Geoid heights at all GPSBMs are synthesized from the GRACE-derived geopotential model GGM03S (converted to tide-free), to degree and order 120, a zero-degree undulation of −41 cm is added to the synthesized values to refer them to the WGS84 ellipsoid, and the result is transformed to NAD83. High-frequency geoid content, based on EGM08 from degree 121 to 2160, is removed from the GPSBMs-derived geoid heights to prevent leakage and aliasing in the filtering described below. The GRACE-synthesized geoid height is then subtracted from the resulting long-wavelength GPSBMs-derived geoid height, which also refers to NAD83. The resulting 18,972 differences are gridded on a $5' \times 5'$ using a moving average with Gaussian weights. This grid is passed through a spherical harmonic analysis to degree and order 50. The resulting harmonics are then used to synthesize the surface shown in Fig. 2. Assuming that the GRACE-derived geoid heights and GPS-derived ellipsoidal heights are free of long-wavelength errors, the trend seen in Fig. 2 is purely due to long-wavelength leveling (NAVD88) errors. Removing these errors from any GPSBM-derived geoid height converts it to one that is unaffected by the 1.3 m long-wavelength slope of NAVD88 from coast to coast. This then provides more insight into the remaining short to intermediate wavelength errors.

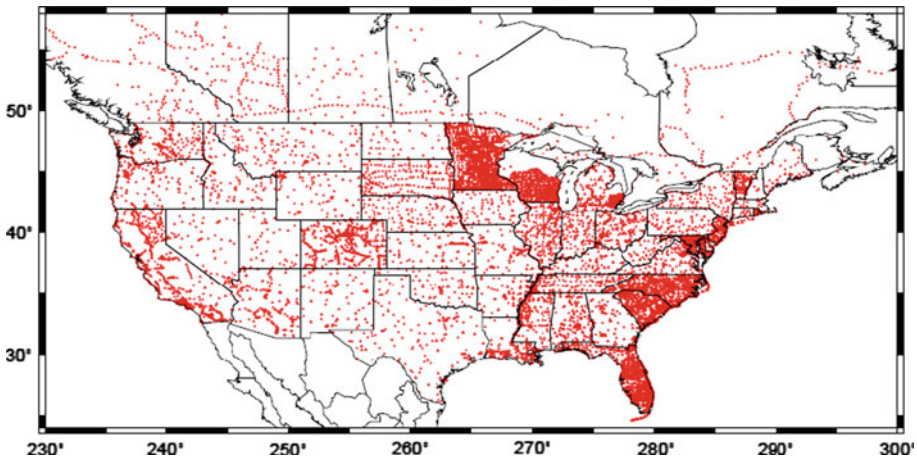

Fig. 1 The 20,446 GPS Bench Marks 2009 (GPSBMs2009)

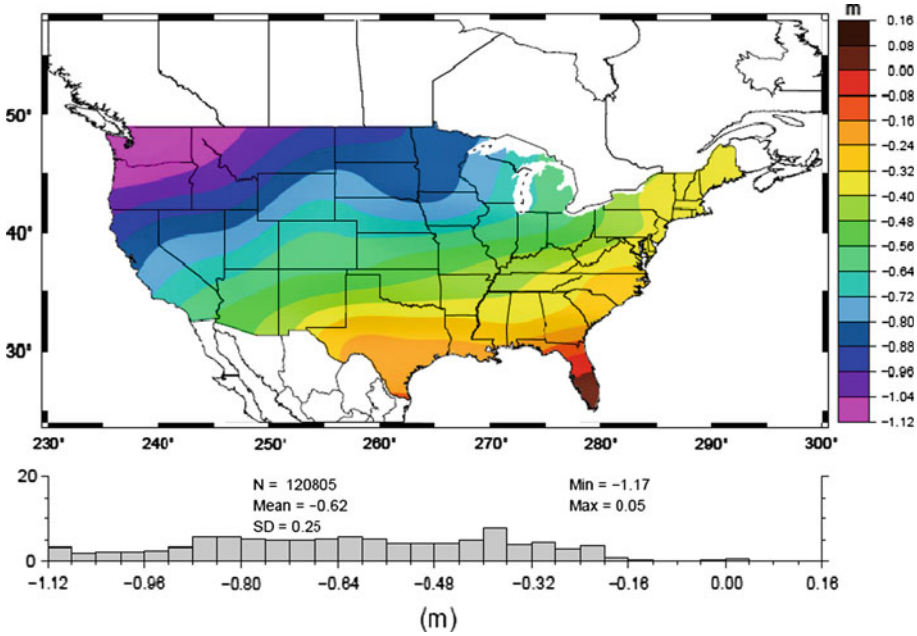

Fig. 2 Long-wavelength errors of the US vertical datum

3. About 200 GPS-occupied tide gauges along the US coastline (Fig. 3).
4. A mean sea surface topography (MSST) model for the Gulf of Mexico (Fig. 4) that is based on purely physical oceanographic principles (based on the Princeton Ocean Model, computed by solving the geostrophic flow equations, but improved by assimilating satellite-derived sea surface temperature and salinity, surface wind and other data). This model is independent of any geoid or tide gauge information (Patchen, 2010, personal communication; Blaha et al. 2000).
5. 3,415 astro-geodetic deflections of the vertical (Fig. 5), which we use to test the deflections derived from USGG2009.

4 Tests and validation

4.1 Comparison to USGG2003

USGG2009 differs significantly from USGG2003 (Fig. 6). The long-wavelength differences are mostly due to the differences between EGM96 and EGM08, but in addition, some differences are due to the erroneous long-wavelength content of the surface and possibly altimetry-derived gravity data, which leaked into USGG2003 through the standard Stokes integral.

There are clear features in the differences associated with the mean sea surface topography of the Gulf Stream and other ocean currents. Improvement on the oceans is mostly

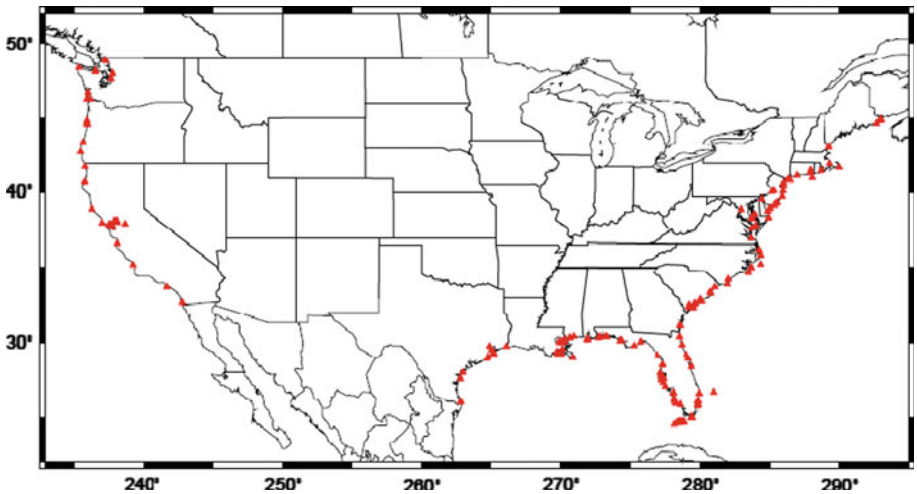

Fig. 3 GPS-occupied tide gauges along the US coastlines

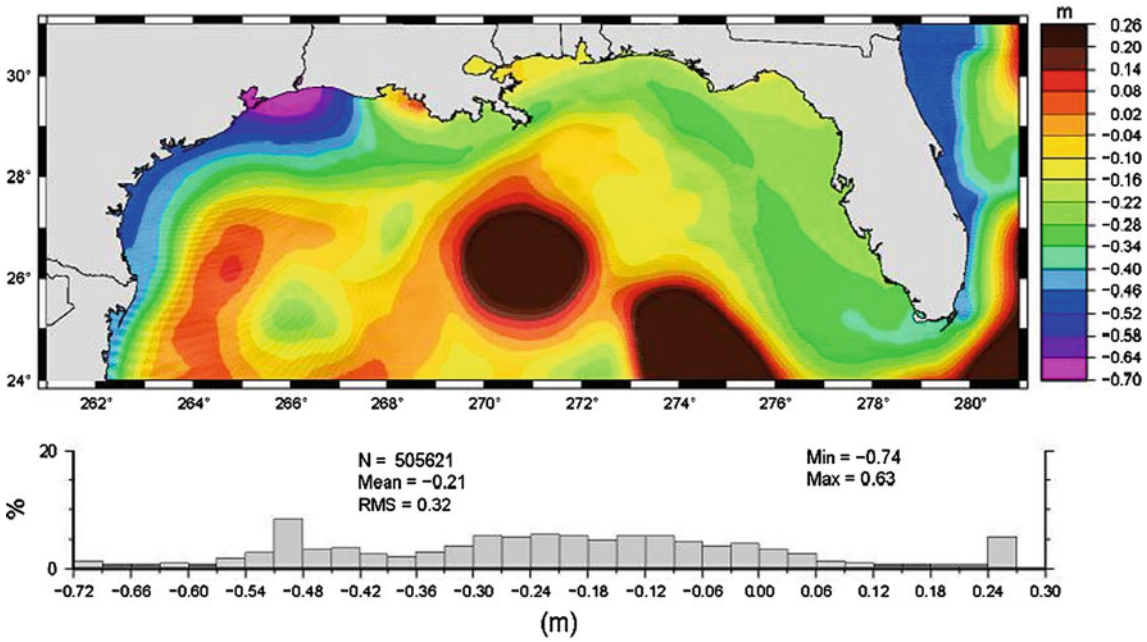

Fig. 4 Mean sea surface topography in the Gulf of Mexico

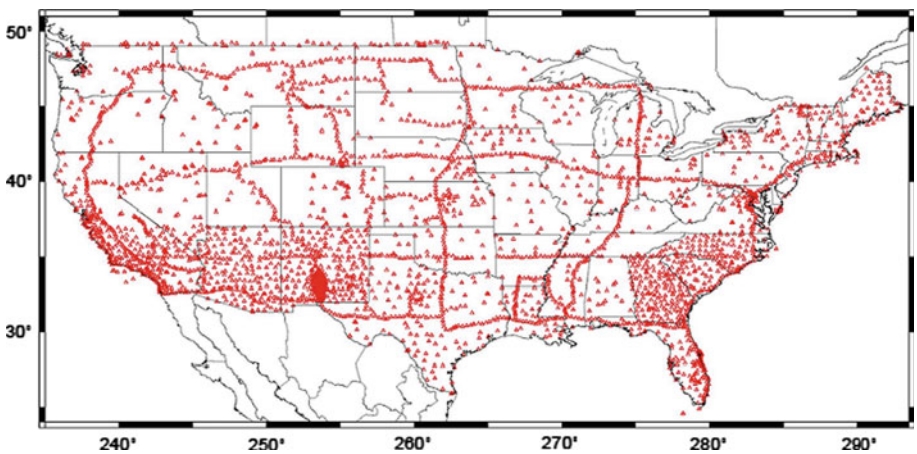

Fig. 5 Locations of 3,415 test astrogeodetic deflections in CONUS

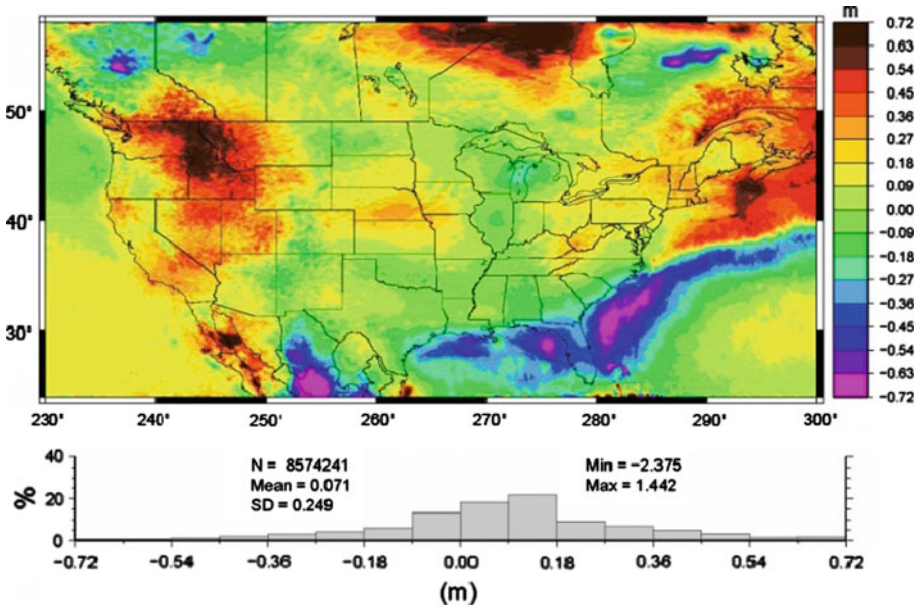

Fig. 6 Difference between USGG2009 and USGG2003

due to better GRACE-derived gravity model incorporated into EGM08. The altimetry data re-tracking (Andersen and Knudsen 2009) improves the gravity recovery and indirectly improves the geoid for the shoreline statistics. In previous models, altimetry data within 20–100 km from the shorelines were edited out. Now gravity data derived from re-tracked altimetry can approach the shoreline. Editing out altimetry-derived gravity near shore does improve the geoid statistics, but only very slightly.

The long-wavelength differences are also due to the inconsistency between the approximate Helmert second condensation method used in USGG2003, and harmonic continuation used in USGG2009. The short-wavelength differences are due to the different gravity data editing criteria, improved topographic data and differences between residual gravity gridding methods.

4.2 Comparison to GPS/leveling-derived geoid heights

USGG2009 geoid heights are compared with those at 18,398 US GPSBMs, after the NSRS2007 adjustment. Each state is compared separately to minimize the effect of long-wavelength errors, which are known to exist in the US vertical datum, NAVD88. Table 1 lists the biases and standard deviations of the differences between USGG2009 and the GPSBMs-derived geoid heights for mountainous states. The nationwide standard deviation of the differences is 6.3 cm while for USGG2003 it is 8.4 cm. The largest improvements occur in northwest CONUS (WA, OR, MT, ID), some Appalachian states (Kentucky, West Virginia, Tennessee) and some topographically flat states of the upper Midwest and western plains (Michigan, Wisconsin, Iowa, Nebraska, North Dakota). Also California, Texas and some southern Rocky states (Arizona, New Mexico, Nevada) improved significantly. Even southeast and northeast states (Florida, South Carolina, North Carolina, New York, Massachusetts, New Hampshire, Vermont and Maine) had some improvements.

The long-wavelength portion of USGG2009 is based on the gravity field as seen by the modern satellite mission GRACE. Consequently, the "bias" of USGG2009, as appears in Table 1, is in fact a bias of the GPSBMs-derived geoid heights due to the long-wavelength errors of NAVD88. This can be seen clearly when comparing the long-wavelength differences between USGG2009 and GPSBMs-derived geoid heights (Fig. 7) to the long-wavelength errors of NAVD88 in Fig. 2. In contrast, USGG2003 is based on the dubious long-wavelength content of the surface and a previous generation altimetry-derived gravity. Figure 8 shows the long-wavelength differences between USGG2003 and the GPSBMs-derived geoid heights. These differences clearly differ from Figs. 2 (and 7) in that they exhibit several local maxima over Washington and Oregon, Idaho, Southern California, South Western Texas, Minnesota, North Dakota and Montana, New England and the Appalachian Mountains. These local maxima most likely represent long-wavelength errors of USGG2003.

4.3 Comparisons with tide gauge-derived geoid heights

The U.S. GPSBMs may not be an entirely appropriate dataset for geoid testing since GPSBMs-derived geoid heights may be contaminated by leveling (NAVD88) errors and possible motions of the bench marks (BMs) with time. The magnitude of these errors is greater than the likely errors being propagated through the gravimetric geoid. Therefore, a second set of test data is introduced, which is independent of NAVD88

Table 1 Statistics in meters of the residuals: gravimetric geoid—GPSBM2009-derived geoid, over CONUS

State	*N*	USGG2009		USGG2003		USGG2009, no kernel truncation		USGG2009, TC	
		Bias	SD	Bias	SD	Bias	SD	Bias	SD
Arizona	227	0.015	0.087	−0.063	0.090	−0.387	0.102	0.026	0.089
California	738	0.234	0.132	0.018	0.160	0.014	0.179	0.242	0.132
Colorado	562	0.106	0.083	0.031	0.075	−0.177	0.107	0.132	0.082
Idaho	97	0.469	0.079	−0.152	0.091	0.176	0.118	0.504	0.089
Kentucky	123	−0.086	0.038	−0.143	0.086	0.015	0.154	−0.087	0.038
Maine	65	−0.144	0.043	−0.385	0.058	−0.642	0.083	−0.155	0.042
Montana	151	0.469	0.091	0.105	0.177	0.228	0.116	0.497	0.124
Nevada	70	0.247	0.089	−0.054	0.135	−0.136	0.116	0.263	0.103
New Mexico	107	−0.103	0.091	−0.081	0.119	−0.423	0.122	−0.093	0.095
North Carolina	1676	−0.226	0.046	−0.146	0.111	−0.096	0.056	−0.224	0.047
Oregon	202	0.523	0.081	0.329	0.183	0.295	0.108	0.525	0.081
South Carolina	1315	−0.221	0.057	−0.073	0.086	0.021	0.037	−0.218	0.055
Tennessee	302	−0.106	0.031	−0.076	0.077	0.133	0.139	−0.106	0.032
Texas	218	−0.257	0.085	−0.153	0.114	−0.265	0.231	−0.247	0.084
Utah	55	0.223	0.090	−0.089	0.092	−0.174	0.082	0.250	0.093
Washington	259	0.610	0.083	0.197	0.158	0.377	0.077	0.614	0.091
Wyoming	101	0.270	0.089	0.036	0.090	−0.066	0.080	0.290	0.103
National mean	18,398		0.063		0.084		0.091		0.064

Only mountainous states are listed

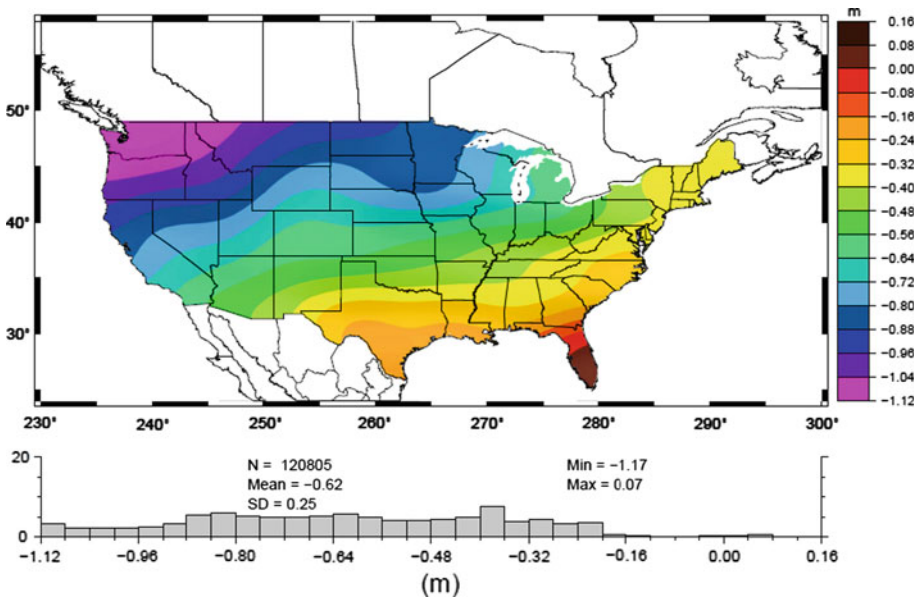

Fig. 7 Long-wavelength differences between USGG2009 and GPSBMs2009

and BMs. This set utilizes GPS-occupied tidal bench marks (TBMs) along the US coast and a MSST model for the Gulf of Mexico that is based on physical oceanographic data and independent of any geoid or tide gauges.

We derive the NAD83 ellipsoidal heights of Mean Sea Level (MSL) at more than 70 TBMs on the Gulf coast, from the Florida Keys to the Mexican border (Fig. 3). This was done by subtracting the vertical distance between the TBM and MSL at the tide gauge, from the TBM's ellipsoidal height relative to NAD83. The geoid at those tide gauges is then computed by subtracting the MSST from the ellipsoidal height of MSL and is compared to USGG2009. Examination of the differences lead to the exclusion of tide gauges in the Florida Keys since the resolution of the MSST model cannot

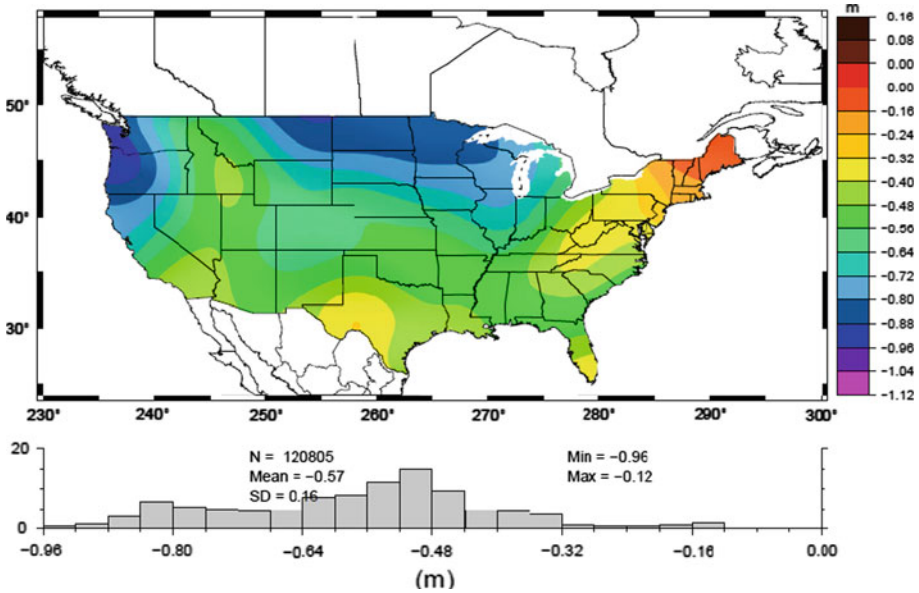

Fig. 8 Long-wavelength differences between USGG2003 and GPSBMs09

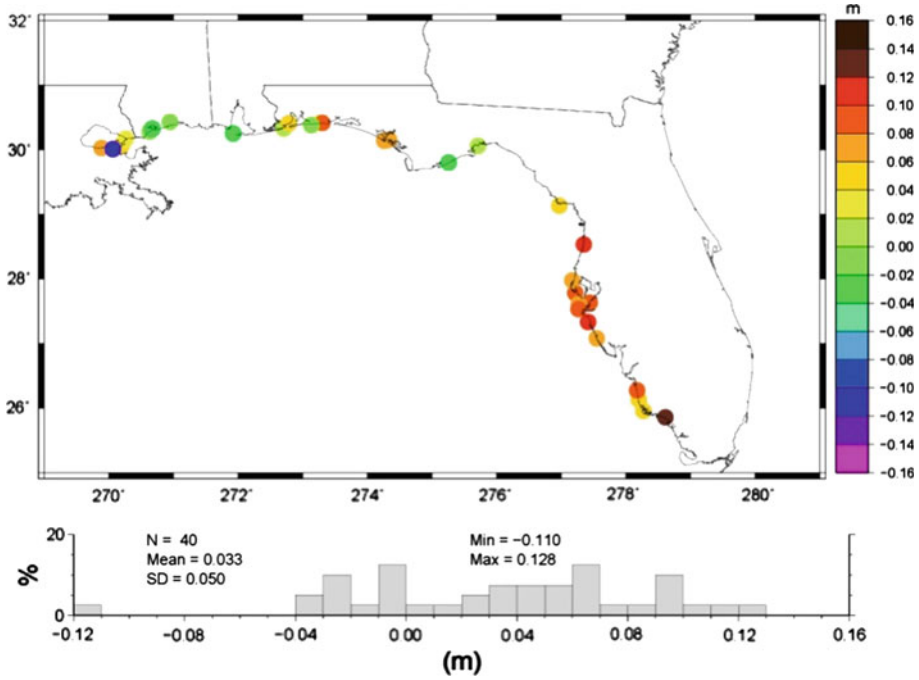

Fig. 9 Difference between USGG2009 and tide-gauge-derived geoid heights

accurately capture the strong effects of the Gulf Stream in the Keys. TBMs in Southeast Louisiana are also excluded to avoid the massive flow from the Mississippi river and subsidence of the coast. Also, all river gauges are excluded to avoid biases due to erroneous MSST near rivers. Finally, all Texas tide gauges were excluded to avoid the effects of winter processes since our MSST model used data from the winter season of 2006. The effect of these processes causes a very low MSST along the Texas coast, as can be seen in Fig. 4 (Patchen, 2010, personal communication).

The remaining 40 Gulf-coast tide gauges are spread over 1000 km, from the tip of Southern Florida to Louisiana. Their derived geoid heights (Fig. 9) are used for comparison with USGG2009, USGG2003 and several other geoid models discussed below (Table 2). The bias of USGG2003 relative to the Gulf's tide gauges is −36 cm while that of USGG2009 is 3 cm. This improvement is due to the accurate long-wavelength contribution of GRACE. It implies that any future changes to W_0 should be minor at most. The standard deviation of the USGG2009 differ-

Table 2 Statistics (in meters) of the differences between 40 Gulf-coast tide-gauge-derived geoid heights and several gravimetric geoid models (see Fig. 9)

Geoid	Statistic			
	Mean	SD	Min	Max
USGG2009	+0.033	0.050	−0.110	+0.128
USGG2003	−0.357	0.085	−0.566	−0.210
USGG2009, no kernel truncation	−0.527	0.079	−0.673	−0.307
USGG2009, TC	+0.025	0.049	−0.118	+0.117

ences is 5 cm, a clear improvement over the 8.5 cm of USGG2003.

4.4 The effect of Stokes' kernel truncation: the long-wavelength content of USGG2009

To test whether the GRACE-derived long-wavelength portion of the field is superior to that contained in the surface and altimetry-derived gravity data, we computed a gravimetric geoid based on the same gravity data and procedures used for USGG2009, but without Stokes' kernel truncation. This "traditional-kernel geoid" is faithful to the long wavelengths of the surface and altimetry-derived gravity in and around North America, rather than that implied by GRACE. The resulting geoid is compared with the GPSBMs09 and tide gauge-derived geoid heights. The statistics of the differences (Tables 1, 2) point clearly in favor of USGG2009, implying that significant long-wavelength errors do contaminate the surface data. Figure 10 shows the difference between USGG2009 and the "traditional kernel geoid". These differences represent, by-and-large, the long-wavelength geoid errors due to the long-wavelength errors of NGS' gravity data and possibly altimetry-derived gravity. These errors cannot be ignored anymore. They are hard to remove by correcting the point gravity data. Rather, they can be easily avoided by a simple truncation of Stokes' kernel at least for that portion of the gravity field signal that satellite gravity missions can observe.

4.5 Harmonic continuation versus approximate Helmert second condensation

We also computed a geoid based on an approximation of Helmert's second condensation method which is based on the Faye gravity anomaly, for comparison and validation of the harmonic continuation method used for USGG2009. The necessary terrain corrections are computed in two parts. The first, the inner-zone contribution, is based on a 3″ DEM and a point-wise integration of the rigorous terrain correction formula (the use of first-order approximation causes spurious results in very steep mountains). The second part, the outer-zone, is based on a global integration of the first-order approximation of the terrain correction formula using a 30″ SRTM and excluding the inner zone contribution.

The resulting geoid is compared with the GPSBMs2009 (Table 1) and TBMs (Table 2). The state-by-state biases are almost identical to those of USGG2009. Although it appears from the overall standard deviation of Table 1 that USGG2009 is slightly better, the Gulf TBMs (Table 2) point in favor of the approximate Helmert second condensation method. However, Table 1 suggests that the harmonic continuation method performs slightly better in the Rocky Mountains (Washington, Idaho, Montana, Wyoming, Utah, Nevada, Arizona and New Mexico). Recall also that the Gulf

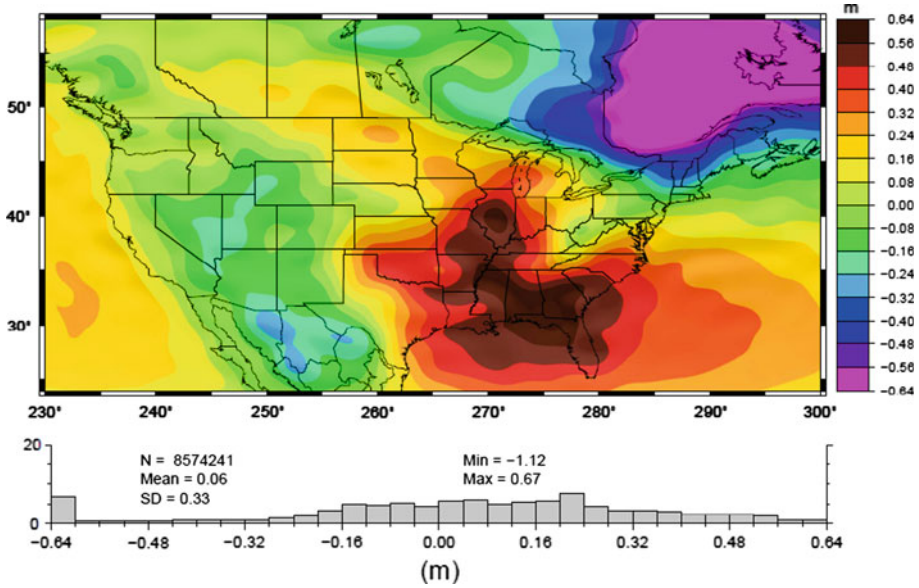

Fig. 10 Estimated long-wavelength geoid errors due to surface and altimetry-derived gravity long-wavelength errors

Coast region, where the tide gauges of Table 2 are located, has a flat topography and a benign gravity signal.

The apparent advantage of the harmonic continuation method could be due to the fact that the Faye anomaly is only an approximation of the Helmert gravity anomaly on the geoid. It may be the case that if the Helmert second condensation method is computed rigorously, it could produce almost identical results to those of the harmonic continuation method. In that case, only one disadvantage of Helmert's second condensation method persists. If the very accurate long-wavelength contribution of GRACE is to overwrite the contribution of the surface gravity data, the reference model must be "Helmertized", which requires a large effort.

4.6 Comparison to EGM08

No matter how good a global geopotential model becomes, it is always possible to design and compute a local geoid with higher frequency content. It is futile, therefore, to compare global with local geoid models for any purpose other than testing the global models. Nevertheless, we present, in Tables 3 and 4, the statistics of the differences between USGG2009 and EGM08 and GPSBMs09 over the US and its territories and comparisons with the tide gauge-derived geoid.

In most of the US and its territories, USGG2009 fits the GPSBMs09 better, sometimes significantly. The EGM08 slightly better fit to the tide gauges in Table 4 is a testimony to its high quality. We repeat, however, that the eastern Gulf coast is a region of flat topography and benign gravity signal. Over most of the Rocky Mountains (New Mexico, Arizona, Nevada, Colorado, Idaho, Wyoming), California and Texas, USGG2009 fits the state-by-state GPSBMs better. EGM08 fits better in Utah and Washington, indicating that the NGS surface gravity data editing in these states should be revisited.

Table 5 presents the statistics of the differences between surface gravimetric deflections of the vertical and 3,415 astro-geodetic deflections in CONUS. The surface gravimetric deflections are computed by applying plumb line curvature corrections to the gravimetric deflections on the geoid (Smith and Roman 2001, Section 8). Strictly speaking, before the comparison can be made, additional corrections should be applied to unify the coordinate systems underlying the astro-geodetic and surface gravimetric deflections. These corrections, however, have a very long-wavelength character and mainly affect the mean of the differences. They change the standard deviations by only a few thousandths of arc second (Jekeli 1999). Since deflections are very high frequency quantities, only the standard deviations are of interest when comparing models. Therefore, we did not apply coordinate system corrections to the data of Table 5. USGG2009 deflections significantly outperform those of EGM08 and the coordinate system corrections cannot really change the picture in any way.

Table 3 Standard deviation (meters) of the differences: gravimetric geoid—GPSBMs09 geoid

Territory	*N*	USGG2009	EGM08
Arizona	227	0.087	0.092
California	738	0.132	0.134
Colorado	562	0.083	0.087
Idaho	97	0.078	0.079
Maine	65	0.043	0.045
Montana	151	0.090	0.089
Nevada	70	0.089	0.091
New Mexico	107	0.091	0.094
North Carolina	1676	0.046	0.047
Oregon	202	0.080	0.080
Tennessee	313	0.031	0.033
Texas	218	0.085	0.088
Utah	55	0.090	0.087
Washington	259	0.083	0.077
Wyoming	101	0.089	0.095
CONUS	18,398	0.063	0.064
Alaska	198	0.275	0.277
Hawaii			
Maui	5	0.028	0.039
Honolulu	17	0.060	0.061
Kauai	6	0.138	0.134
Guam	16	0.045	0.068
North Mariana island			
Saipan	10	0.026	0.033
Tinian	35	0.020	0.017
Rota	9	0.024	0.026
American Samoa	22	0.053	0.112
Puerto Rico and the US Virgin islands	29	0.017	0.030

Table 4 Standard deviation (m) of the differences: gravimetric geoid—tide gauges geoid

Geoid	Statistic				
	n	Mean	SD	Min	Max
USGG2009	40	+0.033	0.050	−0.110	+0.128
EGM08	40	+0.034	0.047	−0.099	+0.123

4.7 The accuracy of USGG2009

The long-wavelength errors of NAVD88 (Fig. 2) are removed from the GPSBM2009-derived geoid heights and compared with USGG2009 and other gravimetric geoid models

Table 5 Mean and standard deviation (″) of the differences between gravimetric and 3,415 observed astro-geodetic deflections of the vertical on the Earth surface in CONUS

Deflection component	USGG2009	EGM08
ξ	Mean = 0.02529	Mean = −0.09113
	SD = 0.87338	SD = 0.97803
	Min = −5.84741	Min = −5.34600
	Max = 5.28829	Max = 5.36200
η	Mean = 0.16115	Mean = 0.18889
	SD = 0.94117	SD = 1.03344
	Min = −5.79390	Min = −5.62400
	Max = 5.91816	Max = 5.97300

(Table 6). We realize that these statistics are still contaminated by tectonic movements affecting the GPSBMs in California and possibly a few other western states and subsidence in Louisiana and Texas. In the rest of the country, the standard deviations of Table 6 are due to USGG2009 errors, but also reflect short-wavelength errors of NAVD88 and ellipsoidal height errors. Based on Table 6, the accuracy of USGG2009 is better than 2–4 cm in flat areas and 5–6 cm in the Rocky Mountains. The extreme values range from −32.1 cm in Washington to 26.4 cm in California.

5 Conclusions

USGG2009 is a new $1' \times 1'$ gravimetric geoid for the US and its territories. It is based on the NGS surface gravity data, DNSC08 altimetry-derived gravity over the oceans, SRTM-DTED1 3″ elevations for its terrain reductions and EGM08 as a reference model.

USGG2009 differs from its predecessors in two major ways: (1) its long-wavelength (>300 km) content is based on GRACE, making its long-wavelength quality significantly better than previous geoid models, and (2) it is computed using the harmonic continuation method rather than the approximate Helmert second condensation with the classical terrain correction.

Validation tests presented in this paper show that this geoid outperforms USGG2003 significantly. These tests indicate that USGG2009 (1) fits the GPS/tide gauge-derived geoid heights to better than 5 cm and a bias of 3 cm implying that any future changes to W_0 should be minor at most, (2) fits the GPSBMs2009 to better than 2–4 cm except in the Rocky Mountains, where it fits to 5–6 cm, provided that the GPSBMs2009 are corrected by removing a GRACE-derived estimate of the NAVD88 long-wavelength errors and (3) Louisiana and Texas are exceptions due to the subsidence of the GPSBMs there. The statistics (Table 6) of California, Washington, Oregon and possibly other western states could be inflated due to tectonics.

Table 6 Statistics of GPSBMs comparisons after removal of long-wavelength error

State	N	USGG2009		USGG2003		USGG2009, No kernel truncation		USGG2009, TC	
		Bias	SD	Bias	SD	Bias	SD	Bias	SD
Arizona	227	0.000	0.048	−0.077	0.100	−0.402	0.059	0.011	0.052
California	738	−0.003	0.058	−0.219	0.087	−0.222	0.099	0.005	0.059
Colorado	562	0.002	0.076	−0.074	0.081	−0.283	0.103	0.027	0.075
Florida	2181	0.000	0.049	0.383	0.074	0.274	0.077	0.011	0.049
Idaho	97	0.008	0.057	−0.613	0.127	−0.285	0.075	0.043	0.063
Maine	65	0.003	0.044	−0.237	0.058	−0.495	0.085	−0.007	0.043
Montana	151	0.026	0.046	−0.339	0.227	−0.216	0.103	0.053	0.073
Nevada	70	0.004	0.054	−0.296	0.106	−0.380	0.065	0.020	0.060
New Mexico	107	−0.022	0.048	0.000	0.065	−0.343	0.097	−0.012	0.049
Oregon	202	−0.004	0.060	−0.198	0.168	−0.232	0.078	−0.002	0.067
Pennsylvania	96	0.026	0.040	−0.113	0.040	−0.210	0.063	0.024	0.039
Rode island	29	0.001	0.023	−0.268	0.026	−0.309	0.027	−0.005	0.024
Tennessee	302	0.013	0.036	0.043	0.065	0.252	0.123	0.013	0.036
Texas	218	−0.008	0.063	0.096	0.128	−0.015	0.221	0.002	0.063
Utah	55	0.015	0.079	−0.297	0.118	−0.384	0.087	0.041	0.076
Washington	259	0.005	0.077	−0.407	0.153	−0.228	0.071	0.009	0.085
Wyoming	101	−0.008	0.064	−0.242	0.155	−0.346	0.089	0.012	0.066
National mean	18,398	0.000	0.043	0.005	0.081	0.013	0.077	0.000	0.044

The iterative process of computing successive gravimetric geoid models seems to have reached an accuracy level of about 5 cm. The contribution of the satellite mission GRACE was monumental in improving the long wavelength of the geoid to reach this level of accuracy. The satellite mission GOCE, which was launched about a year ago, will add some more accuracy to the medium wavelengths of the field, perhaps up to a spatial resolution of 100 km. The journey to arrive at the 1 cm level will depend on improving the existing terrestrial gravity data using aerogravity collected as a part of the Gravity for the Re-definition of the American Vertical Datum (GRAV-D) project and on the improvement of geoid computation methods.

Acknowledgments The authors thank the reviewers for their detailed comments and suggestions. Special thanks to the reviewer with extensive comments which helped to improve the paper.

Appendix

Spherical harmonic expansion of the topography

The spherical harmonic expansion of the powers of elevation, $H^k, k = 1, 2, \ldots$, is needed for the computation of the topographic potential and other quantities required for gravity and topographic reductions.

Global $1' \times 1'$ block means of H, H^2 and H^3 are computed from the SRTM30″ global DEM (Becker et al. 2009), setting all oceanic cells to a nominal height of zero. Each of these three mean grids is then passed through a spherical harmonic analysis using numerical quadrature from degree 0 to 2700.

The geodetic coordinates of each $1' \times 1'$ cell are referenced to the surface of an ellipsoid of a semi-major axis of 6,378,136.3 m and semi-minor axis of 6,356,751.55863 m. Before the spherical harmonic analysis, the geodetic coordinates of each $1' \times 1'$ cell (with $h = 0$) are transformed to geocentric coordinates (geocentric latitude, longitude and radial distance r). The geocentric coordinates, so computed, are adopted for the harmonic analysis as the geocentric coordinates of the $1' \times 1'$ cell.

Computation of quantities related to the topographic reductions

The mathematical derivations in this appendix follow those of Sjöberg (1977). Under the spherical approximation, the topographic potential for the exterior and interior spaces can be expanded into spherical harmonic series as

$$V_{\mathrm{t}}^{\mathrm{e}}(r_P, \mathbf{x}_P) = \sum_{n=0}^{\infty} \left(\frac{R}{r_P}\right)^{n+1} V_n^{\mathrm{e}}(\mathbf{x}_P) \tag{A1}$$

$$V_{\mathrm{t}}^{\mathrm{i}}(r_P, \mathbf{x}_P) = \sum_{n=0}^{\infty} \left(\frac{r_P}{R}\right)^{n} V_n^{\mathrm{i}}(\mathbf{x}_P) \tag{A2}$$

where the subscript "t" stands for the topography, and superscripts "e" and "i" denote the exterior and interior spaces, respectively. Roughly speaking, the exterior and interior spaces are defined as the spaces above and inside the Earth's topography. The surface harmonic functions in (A1) and (A2) are given by

$$V_n^{\mathrm{e}}(\mathbf{x}_P) = \frac{GR^2}{n+3} \sum_{k=1}^{n+3} C_{n+3}^k \hbar^k(\mathbf{x}_P) \tag{A3}$$

$$V_n^{\mathrm{i}}(\mathbf{x}_P) = -\frac{GR^2}{n-2} \sum_{k=1}^{\infty} C_{-(n-2)}^k \hbar^k(\mathbf{x}_P) \tag{A4}$$

The function $\hbar^k$ in (A3) and (A4) can be computed as

$$\begin{aligned} \hbar^k(\mathbf{x}_P) &= \int\!\!\int_{\sigma} \rho \left(\frac{H}{R}\right)^k P_n(\cos\psi)\mathrm{d}\sigma \\ &= \frac{4\pi}{2n+1} \sum_{m=0}^{n} \left[a_{nmk} \overline{R}_{nm}(\mathbf{x}_P) + b_{nmk} \overline{S}_{nm}(\mathbf{x}_P)\right] \end{aligned} \tag{A5}$$

where

$$\begin{pmatrix} a_{nmk} \\ b_{nmk} \end{pmatrix} = \frac{1}{4\pi} \int\!\!\int_{\sigma} \rho \left(\frac{H}{R}\right)^k \begin{pmatrix} \overline{R}_{nm}(\mathbf{x}) \\ \overline{S}_{nm}(\mathbf{x}) \end{pmatrix} \mathrm{d}\sigma, \tag{A6}$$

and where $\overline{R}_{nm}$ and $\overline{S}_{nm}$ are the fully normalized spherical harmonics and H is the orthometric height. A constant density of 2.67 g/cm^3 is used throughout this work.

The series (A3) and (A4) to the fourth power of $\hbar$ are explicitly given by

$$\begin{aligned} V_n^{\mathrm{e}}(\mathbf{x}_P) \approx GR^2 \Bigg[&\hbar + \frac{n+2}{2}\hbar^2 + \frac{(n+2)(n+1)}{6}\hbar^3 \\ &+ \frac{(n+2)(n+1)n}{24}\hbar^4 \Bigg] \end{aligned} \tag{A7}$$

$$\begin{aligned} V_n^{\mathrm{i}}(\mathbf{x}_P) \approx GR^2 \Bigg[&\hbar - \frac{n-1}{2}\hbar^2 + \frac{(n-1)n}{6}\hbar^3 \\ &- \frac{(n-1)n(n+1)}{24}\hbar^4 \Bigg] \end{aligned} \tag{A8}$$

Inserting (A7) and (A8) into Eq. (A1) and (A2), we have

$$V_{\mathrm{t}}^{\mathrm{e}}(r_P, \mathbf{x}_P) = \sum_{n=0}^{\infty} \sum_{m=0}^{n} \left(\frac{R}{r_P}\right)^{n+1} \left(a_{nm}^{\mathrm{e}} \overline{R}_{nm} + b_{nm}^{\mathrm{e}} \overline{S}_{nm}\right) \tag{A9}$$

$$V_{\mathrm{t}}^{\mathrm{i}}(R, \mathbf{x}_P) = \sum_{n=0}^{\infty} \sum_{m=0}^{n} \left(a_{nm}^{\mathrm{i}} \overline{R}_{nm} + b_{nm}^{\mathrm{i}} \overline{S}_{nm}\right) \tag{A10}$$

where

$$\begin{pmatrix} a^{\mathrm{e}}_{nm} \\ b^{\mathrm{e}}_{nm} \end{pmatrix} = \frac{4\pi G R^2}{2n+1} \begin{pmatrix} a_{nm1} + \frac{n+2}{2} a_{nm2} + \frac{(n+2)(n+1)}{6} a_{nm3} + \frac{(n+2)(n+1)n}{24} a_{nm4} \\ b_{nm1} + \frac{n+2}{2} b_{nm2} + \frac{(n+2)(n+1)}{6} b_{nm3} + \frac{(n+2)(n+1)n}{24} b_{nm4} \end{pmatrix} \tag{A11}$$

$$\begin{pmatrix} a^{\mathrm{i}}_{nm} \\ b^{\mathrm{i}}_{nm} \end{pmatrix} = \frac{4\pi G R^2}{2n+1} \begin{pmatrix} a_{nm1} - \frac{n-1}{2} a_{nm2} + \frac{(n-1)n}{6} a_{nm3} - \frac{(n-1)n(n+1)}{24} a_{nm4} \\ b_{nm1} - \frac{n-1}{2} b_{nm2} + \frac{(n-1)n}{6} b_{nm3} - \frac{(n-1)n(n+1)}{24} b_{nm4} \end{pmatrix} \tag{A12}$$

Equations (A9) and (A10) allow for a simple combination of the harmonic coefficients of the expansions of H^k, and then the topographic potential can be evaluated as a standard spherical harmonic series.

If the topography is condensed onto the geoid (Helmert's second condensation), the gravitational potential of the condensed surface layer at point P is (Moritz 1968, Eq. 56)

$$V_C(r_P, \mathbf{x}_P) = GR^2 \int\int_{\sigma} \rho \frac{H}{l} \mathrm{d}\sigma \tag{A13}$$

Enforcing mass conservation requires a density function of the form (e.g., Heck 2003)

$$\rho' = \rho \left(1 + \frac{H}{R} + \frac{1}{3} \left(\frac{H}{R} \right)^2 \right), \tag{A14}$$

and it leads to

$$V_C(r_P, \mathbf{x}_P) = GR^2 \int\int_{\sigma} \rho \frac{H}{l} \left[1 + \frac{H}{R} + \frac{1}{3} \left(\frac{H}{R} \right)^2 \right] \mathrm{d}\sigma \tag{A15}$$

Using the harmonic expansion of $\hbar^k$, the potential of the surface layer can be written as

$$V^C(r_P, \mathbf{x}_P) = \sum_{n=0}^{\infty} \left(\frac{R}{r_P} \right)^{n+1} \sum_{m=0}^{n} \left[a^C_{nm} \overline{R}_{nm}(\mathbf{x}) + b^C_{nm} \overline{S}_{nm}(\mathbf{x}) \right] \tag{A16}$$

where

$$\begin{pmatrix} a^C_{nm} \\ b^C_{nm} \end{pmatrix} = \frac{4\pi G R^2}{2n+1} \begin{pmatrix} a_{nm1} + a_{nm3} + \frac{1}{3} a_{nm3} \\ b_{nm1} + b_{nm3} + \frac{1}{3} b_{nm3} \end{pmatrix} \tag{A17}$$

Under Helmert's second method of condensation, the potential change δV^{e} for the exterior space is

$$\delta V^{\mathrm{e}}(r_P, \mathbf{x}_P) = V^{\mathrm{e}}_{\mathrm{t}}(r_P, \mathbf{x}_P) - V^C(r_P, \mathbf{x}_P) = \sum_{n=0}^{\infty} \sum_{m=0}^{n} \left(\frac{R}{r_P} \right)^{n+1} \left(a_{nm} \overline{R}_{nm} + b_{nm} \overline{S}_{nm} \right) \tag{A18}$$

where:

$$\begin{pmatrix} a_{nm} \\ b_{nm} \end{pmatrix} = \begin{pmatrix} a^{\mathrm{e}}_{nm} - a^C_{nm} \\ b^{\mathrm{e}}_{nm} - b^C_{nm} \end{pmatrix} \tag{A19}$$

The direct (topographic) effect on the gravity anomaly, A, can be computed directly from (A18) using any spherical harmonic synthesis software:

$$A(r_P, \mathbf{x}_P) = -\frac{\partial(\delta V^{\mathrm{e}})}{\partial r} - \frac{2}{r} \delta V^{\mathrm{e}} = \frac{1}{r_P} \sum_{n=0}^{\infty} \sum_{m=0}^{n} \left(\frac{R}{r_P} \right)^{n+1} (n-1) \left(a_{nm} \overline{R}_{nm} + b_{nm} \overline{S}_{nm} \right) \tag{A20}$$

Similarly, the potential change on the geoid is the difference between $V^{\mathrm{i}}_{\mathrm{t}}$ and the potential of the surface layer:

$$\delta V^{\mathrm{i}}(R, \mathbf{x}_P) = V^{\mathrm{i}}_{\mathrm{t}}(R, \mathbf{x}_P) - V^C(R, \mathbf{x}_P) = \sum_{n=0}^{\infty} \sum_{m=0}^{n} \left(c_{nm} \overline{R}_{nm} + d_{nm} \overline{S}_{nm} \right) \tag{A21}$$

where

$$\begin{pmatrix} c_{nm} \\ d_{nm} \end{pmatrix} = \begin{pmatrix} a^{\mathrm{i}}_{nm} - a^C_{nm} \\ b^{\mathrm{i}}_{nm} - b^C_{nm} \end{pmatrix} \tag{A22}$$

Note the difference in the formulation for the exterior and interior spaces. δV^{e} and δV^{i} are not the same.

The indirect effect on the geoid can be computed using Brun's formula:

$$\delta N_{\mathrm{Ind}} = \frac{\delta V^{\mathrm{i}}}{\gamma} \tag{A23}$$

If the topographic potential $V^{\mathrm{e}}_{\mathrm{t}}$ is harmonic downward continued onto the geoid in the same way as the reference model, the potential difference between the real one V^{i} and the continued one on the geoid is then given by

$$\delta V_b(R, \mathbf{x}_P) = V^{\mathrm{i}}_{\mathrm{t}}(R, \mathbf{x}_P) - V^{\mathrm{e}}_{\mathrm{t}}(R, \mathbf{x}_P) = \sum_{n=0}^{\infty} \sum_{m=0}^{n} \left(a^a_{nm} \overline{R}_{nm} + b^a_{nm} \overline{S}_{nm} \right) \tag{A24}$$

where

$$\begin{pmatrix} a^a_{nm} \\ b^a_{nm} \end{pmatrix} = \begin{pmatrix} a^{\mathrm{i}}_{nm} - a^{\mathrm{e}}_{nm} \\ b^{\mathrm{i}}_{nm} - b^{\mathrm{e}}_{nm} \end{pmatrix} \tag{A25}$$

References

Andersen OB, Knudsen P (2009) DNSC08 mean sea surface and mean dynamic topography models. J Geophys Res 114:C11001

Becker JJ, Sandwell DT, Smith WHF, Braud J, Binder B, Depner J, Fabre D, Factor J, Ingalls S, Kim S-H, Ladner R, Marks K, Nelson S, Pharaoh A, Trimmer R, Von Rosenberg J, Wallace G, Weatherall

P (2009) Global bathymetry and elevation data at 30 arc seconds resolution: SRTM30_PLUS. Mar Geod 32(4):355–371

Bjerhammar A (1963) A new theory of gravimetric geodesy. Division of Geodesy, Royal Institute of Technology, Stockholm

Blaha JP, Born GH, Guinasso NL, Herring HJ, Jacobs GA, Kelly FJ, Leben RR, Martin RD, Mellor GL, Niiler PP, Parke ME, Patchen RC, Shaudt K, Scheffner NW, Shum CK, Ohlmann C, Sturges W, Weatherly GL, Webb D, White HJ (2000) Gulf of Mexico ocean monitoring system. Oceanography 13(2):10–17

Forsberg R (1984) A study of terrain reductions, density anomalies and geophysical inversion methods in gravity field modelling. Report 355, Dept of Geod Sci and Surv, Ohio State University, Columbus

Haagmans R, de Min E, van Gelderen M (1993) Fast evaluation of convolution integrals on the sphere using 1D FFT, and a comparison with existing methods for Stokes'integral. Manusc Geod 18: 227–241

Heck B (2003) On Helmert's methods of condensation. J Geod 77: 155–170

Heiskanen WA, Moritz H (1967) Physical geodesy. Freeman, San Francisco

Jekeli C (1999) An analysis of the vertical deflections derived from high-degree spherical harmonic models. J Geod 73(1):10–22

Martinec Z (1998) Boundary-value problems for gravimetric determination of precise geoid. Lecture notes in earth sciences, vol 73. Springer, Berlin, Heidelberg, New York

Martinec Z, Matyska C, Grafarend EW, Vanícek P (1993) On Helmert's 2nd condensation method. Manus Geod 18:417–421

Milbert DG (1991) Computing GPS-derived orthometric heights with the GEOID90 geoid height model. Technical papers of the 1991 ACSM-ASPRS Fall Convention, Atlanta, Oct 28 to Nov 1, 1991. American Congress on Surveying and Mapping, Washington, D.C. pp A46–A55

Moritz H (1968) On the use of the terrain correction in solving Molodensky's problem. Report no. 108, Department of Geodetic Science and Surveying, Ohio State University

Moritz H (1980) Advanced physical geodesy. Herbert Wichmann Verlag, Karlsruhe

Pavlis NK, Holmes SA, Kenyon SC, Factor JK (2008) An Earth gravitational model to degree 2160: EGM08. Presented at the 2008 general assembly of the European Geosciences Union, Vienna, April 13–18, 2008

Pursell D, M Potterfield (2008) NAD 83(NSRS2007) National Readjustment Final Report. NOAA Technical Report NOS NGS 60, U.S. Department of Commerce, National Oceanic and Atmospheric Administration National Ocean Service, Silver Spring, MD

Roman DR, Wang YM, Henning W, Hamilton J (2004) Assessment of the new national geoid height model, GEOID03. In: Proceedings of the American Congress on surveying and mapping 2004 meeting

Sandwell DT, Smith WHF (2009) Global marine gravity from retracked Geosat and ERS-1 altimetry: ridge segmentation versus spreading rate. J Geophys Res 114

Sjöberg LE (1977) On the error of spherical harmonic developments of gravity at the surface of the Earth. Report no. 257, Department of Geodetic Science and Surveying, The Ohio State University

Sjöberg LE (2000) On the topographic effects by the Stokes-Helmert method of geoid and quasi-geoid determinations. J Geod 74(2):255–268

Sjöberg LE (2001) The effect of downward continuation of gravity anomaly to sea level in Stokes formula. J Geod 74:796–804

Sjöberg LE (2003) A solution to the downward continuation effect on the geoid determined by Stokes' formula. J Geod 77:94–100

Sjöberg LE (2007) The topographic bias by analytical continuation in physical geodesy. J Geod 81:345–350

Slater JA, Garvey G, Johnston C, Haase J, Heady B, Kroenung G, Little J (2006) The SRTM data "Finishing" process and products. Photogramm Eng Remote Sens 72(3):237–247

Smith DA, Milbert DG (1999) The GEOID96 high-resolution geoid height model for the United States. J Geod 73:219–236

Smith DA, Roman DR (2001) GEOID99 and G99SSS: one arc-minute models for the United States. J Geod 75:469–490

Tapley B, Ries J, Bettadpur S, Chambers D, Cheng M, Condi F, Gunter B, Kang Z, Nagel P, Pastor R, Pekker T, Poole S, Wang F (2005) GGM02: an improved Earth gravity field model from GRACE. J Geod 79:467–478

Vaníček P, Kleusberg A (1987) The Canadian geoid—Stokesian approach. Manus Geod 12(2):86–98

Vaníček P, Martinec Z (1994) Stokes-Helmert scheme for the evaluation of a precise geoid. Manus Geod 19(2):119–128

Vaníček P, Najafi M, Martinec Z, Harrie L, Sjöberg LE (1996) Higher-degree reference field in the generalized Stokes-Helmert scheme for geoid computation. J Geod 70:176–182

Wang YM (1990) The effect of topography on the determination of the geoid using analytical downward continuation. Bull Geod 64(3):231–246

Wang YM (1997) On the error of analytical downward continuation of the earth's external gravitational potential on and inside the earth's surface. J Geod 71:70–82

Wang YM (2001) GSFC00 mean sea surface, gravity anomaly, and vertical gravity gradient from satellite altimeter data. J Geophys Res 106(C12):31167–31174

Wang YM, Rapp RH (1990) Terrain effects on geoid undulation computations. Manus Geod 15(1):23–29

Wong L, Gore R (1969) Accuracy of geoid heights from modified Stokes kernels. Geophys J R Astr Soc 18:81–91